Available online at www.sciencedirect.com
ScienceDirect
Chemical Physics Letters 455 (2008) 103–109
CHEMICAL PHYSICS LETTERS
www.elsevier.com/locate/cplett

Analytical representation of the Becke–Roussel exchange functional

Emil Proynov, Zhenting Gan, Jing Kong *

Q-Chem Inc., The Design Center, Suite 690, 5001 Baum Boulevard, Pittsburgh, PA 15213, USA

Received 30 November 2007; in final form 13 February 2008
Available online 19 February 2008

Abstract

The unique meta-GGA (generalized gradient approximation) exchange functional of Becke and Roussel (BR89) and the correlation functional of Becke related to it (B94) are represented for the first time in an analytical form. All functional derivatives are then obtained analytically, which allows an efficient self-consistent implementation. A brief assessment of this 'BR89B94' meta-GGA scheme is made considering molecular atomization energies and equilibrium geometries, with the latter being reported for the first time. The hybrid version of it yields one of the most accurate atomization energies to date, but its bond distances are less satisfactory. Some interesting features of the BR exchange hole are discussed.

1. Introduction

The Becke–Roussel (BR89) exchange functional [1] has attracted attention recently in Kohn–Sham density functional theory (KS-DFT) in relation to the real-space post-Hartree–Fock-DFT approach to the non-dynamical correlation [2,3], and the DFT model of van der Waals interactions [4]. Its accurate performance has been established to some extent earlier [1,5]. The model is based on the following ansatz for the spherically averaged exchange hole (negatively defined here)

$$\bar{h}_X(a,b;s) = -\frac{a}{16\pi bs}\left[(a|b-s|+1)\mathrm{e}^{-a|b-s|} - (a|b+s|+1)\mathrm{e}^{-a|b+s|}\right], \quad (1)$$

where a, b are positive, position-dependent parameters and s is the inter-electronic distance. This ansatz originates from the form of the exchange hole of hydrogen atom. It provides the required normalization of the hole for any positive values of a and b:

$$4\pi\int_0^\infty \bar{h}_{X\sigma}(a,b;s)s^2\,\mathrm{d}s = -1. \quad (2)$$

It is plausible to assume that in atomic and molecular systems the exchange hole would resemble that of the hydrogen atom, which implies some degree of universality of this hole. A similar idea was explored also in the work of Gill and Pople [6]. This is in contrast to the alternative universality hypothesis that is behind the local spin density approximation (LSD) starting from a very different limit, the uniform electron gas.

The two parameters a and b are used so as to obey the known value and curvature of the spherically averaged exact exchange hole at small s [1]

$$\bar{h}_{X\sigma}(\mathbf{r},0) = -\rho_\sigma(\mathbf{r}),$$
$$\bar{h}_{X\sigma}(\mathbf{r},s)|_{s\to 0} = -\rho_\sigma(\mathbf{r}) - Q_\sigma(\mathbf{r})s^2, \quad (3)$$
$$Q_\sigma(\mathbf{r}) = \frac{1}{6}\left[\nabla^2\rho_\sigma(\mathbf{r}) - 2D_\sigma(\mathbf{r})\right],$$
$$D_\sigma = 2\tau_\sigma - \frac{1}{4}\frac{|\nabla\rho_\sigma|^2}{\rho_\sigma}, \quad (4)$$

where ρ_σ is the electron density of spin σ, $\mathbf{r}$ is the co-ordinate vector of the reference electron. These properties are provided when the parameters a and b obey the following system of equations:

$$a^3\mathrm{e}^{-ab} = 8\pi\rho_\sigma, \quad (5)$$
$$a^2b - 2a = \frac{6bQ_\sigma}{\rho_\sigma}. \quad (6)$$

* Corresponding author.
E-mail address: jkong@q-chem.com (J. Kong).

0009-2614/$ - see front matter © 2008 Elsevier B.V. All rights reserved.
doi:10.1016/j.cplett.2008.02.039

The above conditions lead to a specific nonlinear equation for x in a spin-resolved form with $x = ab$ ($x \geqslant 0$) [1]

$$\frac{x_\sigma e^{-2x_\sigma/3}}{(x_\sigma - 2)} = y_\sigma(x) \equiv \frac{2}{3}\pi^{2/3}\frac{\rho_\sigma^{5/3}}{Q_\sigma}. \tag{7}$$

Solving this equation at each reference point gives the function x_σ which in turn determines uniquely the exchange hole, the exchange energy (E_X) and the corresponding Slater potential

$$E_X = \frac{1}{2}\sum_\sigma \int_{\infty^3} \rho_\sigma(\mathbf{r}) U_{X\sigma}(\mathbf{r})\, d\mathbf{r}, \tag{8}$$

$$U_{X\sigma}(\mathbf{r}) = 4\pi \int_{\infty^3} s\, ds \bar{h}_{X\sigma}(\mathbf{r}, s) = -2\pi^{1/3}\rho^{1/3}\left(\frac{e^{x_\sigma/3}}{x_\sigma}\right)\left[1 - e^{-x_\sigma} - \frac{1}{2}x_\sigma e^{-x_\sigma}\right]. \tag{9}$$

Eq. (7) is a complicated nonlinear equation and can only be solved numerically at each reference point, as suggested by Becke and Roussel [1]. Similar problem arises in the post-Hartree–Fock real-space correlation (RSC) model of Becke [2,3], where the shape of the BR exchange hole is used as an auxiliary function in a different context. For the latter, Arbuznikov and Kaupp [7] have proposed recently an analytical interpolation that avoids solving a nonlinear equation. However, the original BR exchange functional was not considered in their work. With this in mind, we present here a detailed analysis of the function $x(y)$ used in the original functional [1]. We will derive an analytical interpolation of $x(y)$ of high accuracy that will be used to achieve a convenient self-consistent implementation of the BR exchange functional. Some interesting features of the BR exchange hole will be noted in passing.

2. Analytical interpolation of the BR functional

The original BR exchange model is based on solving the nonlinear Eq. (7) numerically for the unknown function $x(y)$. The inverse function $y(x)$, depicted in Fig. 1, is known, defined by Eq. (7) via the electron density and the exchange hole curvature. It consists of two pieces delineated by a discontinuity point at $x = 2$. The lower piece of $y(x)$ is located in the negative range of y for $0 \leqslant x < 2$ and has the following asymptotic form:

$$\lim_{x\to 0} y(x) \to -\frac{1}{2}x + \frac{1}{12}x^2, \tag{10}$$

$$\lim_{x\to 2} y(x) \to e^{-4/3}\left[\frac{2}{x-2} - \frac{1}{3} - \frac{2}{9}(x-2)\right] \to -\infty. \tag{11}$$

The upper piece of $y(x)$ is positive for $2 < x \leqslant \infty$, and tends to $+\infty$ by the same Eq. (11) when x approaches the singular point $x = 2$ from above. When x goes to plus infinity, the upper piece of $y(x)$ tends to zero as

$$\lim_{x\to+\infty} y(x) \to e^{-2x/3}\left[1 + \frac{2}{x} + \frac{4}{x^2}\right]. \tag{12}$$

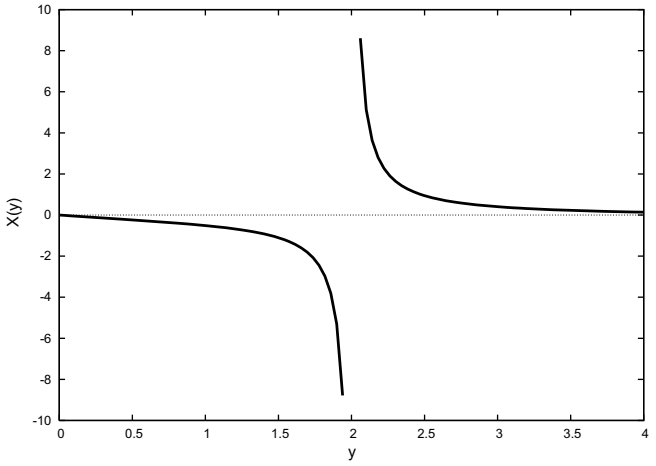

Fig. 1. The starting function $y(x)$ defined via Eq. (7). This function is discontinuous at $x = 2$.

Eq. (7) can be solved numerically with respect to x on a grid of points along the y-axis, and the shape of $x(y)$ can be envisaged numerically as in Fig. 2. Meaningful are only positive values of $x(y)$. Similar to $y(x)$, the function $x(y)$ consists of two pieces in the positive domain, delineated by a point of discontinuity at $y = 0$. Both pieces tend to the same limit of $x = 2$ when y tends to either minus infinity (the lower piece) or to plus infinity (the upper piece). This situation is rather different from the interpolation problem considered in Ref. [7]. Their function is continuous with no singularities. In our case, the function $x(y)$ resembles the inverse hyperbolic function arccsch(y) to some extent. A more detailed analysis revealed that only the upper piece of $x(y)$ located in $0 \leqslant y \leqslant +\infty$ can be accurately interpolated by a properly shifted arccsch(x) function, as described further on.

In previous studies of the BR model [1,5,7], it was presumed that the variable y can be both positive or negative, for there is always a positive solution for $x(y)$ in the whole

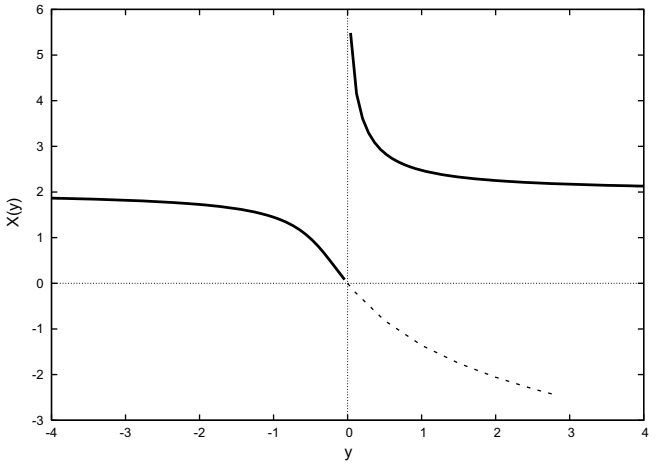

Fig. 2. The required function $x(y)$ constructed from numerical estimates. The point of discontinuity at $y = 0$ is also a branching point.

range of $-\infty \leqslant y \leqslant +\infty$ [1]. The curvature of the BR exchange hole is given by $-Q$ (from Eq. (3)). It is positive when the (negatively defined) hole is well localized around the reference point. In such cases the hole has a single minimum at the reference point where y is negative (Q is negative) and $x(y)$ is confined in the range $0 \leqslant x \leqslant 2$ (i.e. in the lower piece). When the curvature is negative (positive Q), the exchange hole has a local maximum at the reference point and a sphere (shell) of local minima around it at a certain distance (in 3D view). These features of the BR exchange hole are clearly discerned from Fig. 2 of Ref. [1] on the example of the neon atom: the transition from a positive curvature to a negative curvature of the exchange hole at the reference point occurs when the reference electron is brought far enough from the nucleus [1]. Having the function $x(y)$ in its lower piece where the hole curvature is positive is a rather different situation from having $x(y)$ in its upper piece where the hole curvature is negative. This difference is especially pronounced at small and vanishing values of $|y|$, close to the point of discontinuity $y = 0$. We have verified that $x(y)$ remains finite in its upper piece for any arbitrary small but non-zero value of y. Such a behavior resembles the function arccsch(x). In the vicinity of $y \approx -0$ the lower piece of $x(y)$ decreases much faster when y vanishes than $x(y)$ grows for $y \approx +0$ in its upper piece.

There is a second branch of $x(y)$ located in the positive range of y, but in the physically forbidden negative domain of $x(y)$ as shown on Fig. 2. The point $y = 0$ is therefore also a branching point for the solutions of the nonlinear Eq. (7). At this branching point the topology of the exchange hole changes drastically. The two positive pieces of $x(y)$ require therefore separate interpolation procedures. Recall that the lower piece is in the range $0 \leqslant x \leqslant 2$, for $-\infty \leqslant y \leqslant 0$. By inverting the asymptotic expansion of $y(x)$ at small x, Eq. (10), we obtain the following exact asymptotic limit of $x(y)$ that is accurate for $-0.1 \leqslant y \leqslant 0$:

$$\lim_{y\to-0} x(y) \to 3 - \sqrt{9 + 12y} \to 0. \tag{13}$$

In the opposite limit when y tends to $-\infty$, we obtain the following exact asymptotic form that yields accurate estimations in the range $-\infty \leqslant y \leqslant -2$:

$$\lim_{y\to-\infty} x(y) \approx \frac{5}{4} - \frac{9}{4} y e^{4/3} - \frac{3}{4}\sqrt{17 + 6ye^{4/3} + 9y^2 e^{8/3}} \to 2. \tag{14}$$

To facilitate the analytical differentiation of the BR functional, it is desirable to approximate each piece of $x(y)$ with one single function. Following some reverse analogy with the problem considered in Ref. [7], we have found that the following trigonometric ansatz is quite suitable for the lower piece of $x(y)$:

$$x(y) = -\arctan(a_1 y + a_2) + a_3, \quad -\infty \leqslant y \leqslant 0, \tag{15}$$

where the coefficients a_i are fitting constants. Those were optimized by solving numerically several systems of equations with respect to a_i generated by Eq. (15) at various wisely selected points of y. We achieved a further improvement in accuracy by employing in addition a modulating factor $f(y)$:

$$x(y) = [-\arctan(a_1 y + a_2) + a_3] f(y), \quad -\infty \leqslant y \leqslant 0. \tag{16}$$

The factor $f(y)$ is optimized in a secondary optimization loop using the Thiele interpolation formula of continued fractions [8]. The corrections from this factor are important mainly in the region of small $|y|$. The final form of our analytical representation of $x(y)$ in its lower piece reads

$$\begin{aligned} x(y) &= g(y)\frac{P_1(y)}{P_2(y)}, \quad -\infty \leqslant y \leqslant 0, \\ g(y) &= -\arctan(a_1 y + a_2) + a_3, \end{aligned} \tag{17}$$

where $P_i(y)$ are fifth order polynomials

$$P_1(y) = \sum_{i=0}^{5} c_i y^i; \quad P_2(y) = \sum_{i=0}^{5} b_i y^i. \tag{18}$$

The optimal values of the coefficients a_i, b_i and c_i in Eqs. (17) and (18) obtained in this work are given in Appendix. This form of $x(y)$ has asymptotic expansions that match closely the values of the exact asymptotic relations in Eqs. (13) and (14)

$$\lim_{y\to-0} x(y) = -1.999977y + 0.663026y^2 + 0.482251y^3, \tag{19}$$

$$\lim_{y\to-\infty} x(y) = 2 + \frac{1}{y}0.527194 - \frac{1}{y^2}0.046324. \tag{20}$$

Results with this form of $x(y)$ and the exact solution are presented in Table 1, with y values sampled in a wide range. One can see that the analytical fit provides a high accuracy with mean-absolute-deviation (MAD) $= 7.73 \times 10^{-7}$, and mean-absolute-percentage-deviation (MAPD) $= 0.0005\%$.

The upper piece of $x(y)$ is located in the positive domain $0 < y \leqslant +\infty$, where $x(y)$ is bound from below by a limit of $x \geqslant 2$ (Fig. 2). By inverting the asymptotic expansion of $y(x)$ when x tends to 2 from above, Eq. (11), we obtain the following exact asymptotic form of $x(y)$ in its upper piece, accurate within the range $2 \leqslant y \leqslant +\infty$:

$$\lim_{y\to+\infty} x(y) \approx \frac{5}{4} - \frac{9}{4} y e^{4/3} + \frac{3}{4}\sqrt{17 + 6ye^{4/3} + 9y^2 e^{8/3}} \to 2. \tag{21}$$

Note that $x(y)$ has a discontinuity at $y = 0$ here and we were not able to obtain analytically its asymptotic expansion in this limit. We have found that this piece of $x(y)$ can be very well approximated by a shifted arccsch(x) function, as it has similar form and behavior at small y. To achieve an even higher accuracy we have employed again a modulating factor $f(y)$ that is optimized in a secondary optimization loop similarly to the lower piece of $x(y)$, Eq. (16). The final form of our analytical representation of the upper piece of $x(y)$ is

Table 1
Comparison of exact vs interpolated values of the function $x(y)$

$y<0$	Exact $x(y)$	Fitted $x(y)$[a]	$y>0$	Exact $x(y)$	Fitted $x(y)$[b]
−0.001	0.000200007	0.000200004	0.0001	14.045919490	14.045919490
−0.01	0.020065982	0.020065542	0.001	10.672890134	10.672890134
−0.1	0.205805180	0.205805180	0.1	4.3713083907	4.3713083907
−0.5	0.980143530	0.980143530	0.5	2.8520020822	2.8520020822
−1.0	1.448513440	1.448513440	1.0	2.4752876179	2.4752876179
−2.0	1.726947198	1.726947198	3.0	2.1702309340	2.1702315305
−4.0	1.865532967	1.865532967	5.0	2.1035015269	2.1035015269
−8.0	1.933402964	1.933402964	8.0	2.0651537106	2.0651535646
−10.0	1.946830450	1.946830450	10.0	2.0522448435	2.0522448435
−100.0	1.994723437	1.994723443	100.0	2.0052672984	2.0052695780
MAD[c]		7.73×10^{-7}			4.11×10^{-7}
MAPD		0.0005%			2.03×10^{-5}%

[a] Interpolation of the lower piece of $x(y)$, Eqs. (17) and (18).
[b] Interpolation of the upper piece of $x(y)$, Eqs. (22) and (23).
[c] The mean absolute errors are from a larger number of values than presented in the table.

$$x(y)=\tilde{g}(y)\frac{\widetilde{P}_1(y)}{\widetilde{P}_2(y)},\quad 0<y\leqslant+\infty, \tag{22}$$
$$\tilde{g}(y)=\operatorname{arccsch}(By)+2,\quad B=2.085749716493756,$$

where the modulation factor is again a ratio of two polynomials

$$\widetilde{P}_1(y)=\sum_{i=0}^{5}d_iy^i;\quad \widetilde{P}_2(y)=\sum_{i=0}^{5}e_iy^i, \tag{23}$$

The optimal coefficients in Eq. (23) obtained in this work are given in the Appendix.

The results from this interpolation have a MAD = 4.11×10^{-7} and MAPD = 2.03×10^{-5}. In our final implementation of the BR model we use Eqs. (22) and (23) for the upper piece of $x(y)$, and Eqs. (17) and (18) for the lower piece.

Finding an accurate analytical representation of the function $x(y)$ is beneficial not only for the BR89 exchange functional. Becke has developed also an efficient meta-GGA correlation functional (B94) [9] which utilizes the BR89 exchange functional. The correlation energy density of B94 is a sum of opposite-spin and parallel-spin components, each derived separately

$$\varepsilon_c^{\mathrm{opp}}=-0.8\rho_\alpha\rho_\beta z_{\alpha\beta}^2\left[1-\frac{\ln(1+z_{\alpha\beta})}{z_{\alpha\beta}}\right], \tag{24}$$
$$\varepsilon_c^{\mathrm{par}}=\varepsilon_c^{\alpha\alpha}+\varepsilon_c^{\beta\beta},\quad \varepsilon_c^{\sigma\sigma}=-0.01\rho_\sigma D_\sigma z_{\sigma\sigma}^4\left[1-\frac{2}{z_{\sigma\sigma}}\ln\left(1+\frac{z_{\sigma\sigma}}{2}\right)\right], \tag{25}$$

where D_σ is the τ-dependent term entering the expression of the exact exchange hole curvature, Eq. (4), and $z_{\sigma\sigma'}$ are spin-dependent correlation lengths defined from physical arguments [9]

$$z_{\alpha\beta}=0.63(R_{\mathrm{F}}^{\alpha}+R_{\mathrm{F}}^{\beta});\quad z_{\sigma\sigma}=1.76R_{\mathrm{F}}^{\sigma}, \tag{26}$$
$$R_{\mathrm{F}}^{\sigma}=-\frac{1}{U_{X\sigma}}. \tag{27}$$

$U_{X\sigma}$ is the exchange energy density of the BR89 exchange functional given as a function of x_σ by Eq. (9). Thus, the function $x(y)$ governs both the BR89 exchange and the B94 correlation functionals in a complicated manner. Results from this particular meta-GGA exchange–correlation scheme, BR89B94, were reported so far only in Ref. [9] but within a post-LDA implementation using a numerical solution for $x(y)$. Later on Neumann et al. [5] studied the BR89 exchange in combination with the P86 GGA correlation functional [10] in a SCF manner, again with a numerical solution for $x(y)$. The analytical representation of the BR89B94 functional allows exploring its full capabilities, including the efficient calculation of the SCF energy and its gradients with respect to nuclear motions. It also avoids potential instabilities associated with numerical solutions, particularly for small argument values.

3. Preliminary results and discussion

We have first examined the accuracy of our analytical interpolation on a set of nine atoms and nine molecules at their experimental geometries. All calculations were done with the Q-Chem program, 3.1 release [11]. The G3 theory basis set G3LARGE [12,13] and an unpruned grid consisting of 128 radial and 194 angular points were employed. All functionals considered, including the meta-GGA ones, are implemented in a fully SCF manner in the way described in Ref. [14]. Table 2 compares total electronic energies, their separate exchange and correlation components and atomization energies obtained with the BR89B94 functional with either analytical or numerical resolution for the function $x(y)$. A very good agreement between the two algorithms is systematically observed, with MAD for total electronic energies of 6.7×10^{-5} a.u. Energy differences like atomization energies differ by only a fraction of a kcal/mol. We compare our results also with the original BR89B94 values reported in Ref. [9]. The agreement on average is good (with CN having the largest error) considering that Becke and Roussel have used a

Table 2
Total energy components ($-1 \times$ a.u.) and atomization energies D_e (kcal/mol, no ZPE) obtained with, and without the analytical representation of BR89B94

		PW[a]	PW[b]	BR[c]	Exact[d]
He	E_X	1.03415	1.03419	1.039	1.026
	E_c	0.041372	0.041370	0.042	0.042
	E_{tot}	2.91780	2.91786		
Ne	E_X	12.14603	12.14607	12.19	12.11
	E_c	0.36242	0.36242	0.365	0.390
	E_{tot}	128.98224	128.98227		
Ar	E_X	30.06283	30.06289	30.09	30.19
	E_c	0.72806	0.72805	0.730	0.722
	E_{tot}	527.45448	527.45457		
C	E_X	5.08154	5.08187		
	E_c	0.15332	0.15343	0.160	0.151
	E_{tot}	37.86761	37.86791		
N	E_X	6.61396	6.61406		
	E_c	0.18879	0.18878	0.192	0.185
	E_{tot}	54.62044	54.62054		
O	E_X	8.22177	8.22182		
	E_c	0.24393	0.24392	0.259	0.248
	E_{tot}	75.10364	75.10370		
F	E_X	10.05262	10.05266		
	E_c	0.302997	0.302994	0.315	0.318
	E_{tot}	99.77505	99.77509		
S	E_X	24.94265	24.94268		
	E_c	0.600913	0.600909	0.615	0.597
	E_{tot}	398.07699	398.07704		
Cl	E_X	27.42032	27.42036		
	E_c	0.664233	0.664227	0.675	0.658
	E_{tot}	460.09049	460.09055		
H_2	E_X	0.66006	0.66010		
	E_c	0.036973	0.036971		
	E_{tot}	1.17274	1.17278		
	E_{at}	106.88	106.88	107.5	109.54
CN	E_X	11.76242	11.76244		
	E_c	0.409094	0.409091		
	E_{tot}	92.78074	92.78079		
	E_{at}	183.67	183.45	186.03	181.03
N_2	E_X	13.27693	13.27696		
	E_c	0.464382	0.464377		
	E_{tot}	109.60537	109.60543		
	E_{at}	228.73	228.64	227.1	228.53
NO	E_X	14.82875	14.82879		
	E_c	0.503080	0.503076		
	E_{tot}	129.97349	129.97353		
	E_{at}	156.51	156.44	156.3	152.9
H_2O	E_X	9.01348	9.01352		
	E_c	0.324425	0.324423		
	E_{tot}	76.47354	76.47358		
	E_{at}	230.60	230.56	230.42	232.22
CH_4	E_X	6.62480	6.62484		
	E_c	0.28180	0.28179		
	E_{tot}	40.53071	40.53076		
	E_{at}	413.06	412.87	413.3	419.25
CH_3OH	E_X	14.95799	14.95804		
	E_c	0.569564	0.569560		
	E_{tot}	115.78243	115.78248		
	E_{at}	505.99	505.75	504.2	511.95
NH_3	E_X	7.72389	7.72394		
	E_c	0.304246	0.304242		
	E_{tot}	56.58877	56.58881		
	E_{at}	291.60	291.54	292.2	297.49
HCN	E_X	12.20263	12.20266		
	E_c	0.445280	0.445275		
	E_{tot}	93.49043	93.49048		
	E_{at}	314.49	314.26	313.2	311.78

[a] Present work with the analytical interpolation of $x(y)$, MAD(E_{tot}) = 6.7×10^{-5} a.u.
[b] Present work with numerical solution for $x(y)$.
[c] Results from Refs. [1,9] with the original BR89B94 scheme.
[d] The exact E_c's of atoms are from Ref.[15] based on exact Kohn–Sham exchange reference, rather than Hartree–Fock reference. The experimentally derived ('exact') values of D_e used in this work are obtained by a careful compilation of the data from Refs. [16,17].

numerical basis [1] whereas we have used Gaussian basis set. Other differences between the two sets of results include the numerical quadratures, and possibly slightly different bond lengths used. We use here experimental geometries corrected for ro-vibrational effects as recommended in Ref. [18]. Also to keep in mind that Ref. [9] presents only D_o from which we have obtained the corresponding BR values of D_e by subtracting the experimentally derived zero-point vibrational contribution.

Next, we calculated a set of atomization energies and equilibrium geometries (Table 3) obtained using the analytical representation of the BR89B94 functional. The compact test set described in Refs. [19,14] was used in part here: carefully selected 20 diatomic molecules and 19 small to medium size polyatomic molecules:

H_2, N_2, F_2, O_2, S_2, P_2, Cl_2, HF, CO, NO, PN, CN, NH, CS, CH, OH, HCl, SiO, NaCl, NaF, HCN, H_2O, H_2S, CO_2, NH_3, PH_3, N_2O, H_2O_2, SiH_4, CH_4, C_2H_2, C_2H_4, C_2H_6, H_2CO, CH_3OH, C_6H_6, C_4H_6 (trans-butadiene), C_4H_5N (pyrrole), C_5H_5N (pyridine).

About one third of these molecules are difficult cases at least at GGA level of DFT. Such a test composition allows more distinct comparison between different functionals. Using a very large set of molecules with a small fraction of 'difficult' cases would be less informative [19]. Results from some popular functionals, BLYP [20,21], BtLap [20,14], B3LYP [22,23], BMK [24], M06 [25,26], are also given in Table 3 for comparison. All atomization energies D_e are computed at the respective optimized geometries. Since there are some slight differences in the exact values referred to in the literature, we summarize in Table 4 the exact atomization energies and bond lengths used here after a careful analysis and compilation of various experimental and theoretical literature data [16–18,27,28].

Comparing the absolute mean errors (MAE) for atomization energies D_e, the performance of the BR89B94 scheme is of about the same accuracy as BLYP, both having

Table 3
Mean absolute errors (MAE) for atomization energies D_e (kcal/mol, no ZPE) of 39 molecules, and MAE for bond lengths R_e (Å) in 36 molecules (45 bonds)

MAE for D_e			
	20 diatomics	19 polyatomics	All 39 molecules
XC with no HF exchange			
BLYP	5.58	5.23	5.41
BtLap	3.08	3.81	3.44
BR89B94	3.60	7.32	5.41
XC with HF exchange			
BMK	2.72	2.49	2.61
M06	2.69	2.57	2.63
B3LYP	2.51	1.82	2.17
$BR89B94_{hyb}$	1.67	2.09	1.87

MAE for R_e			
	Diatomics	Polyatomics	All 45 bonds
XC with no HF exchange			
BLYP	0.0174	0.0112	0.0140
BtLap	0.0155	0.0105	0.0127
BR89B94	0.0335	0.0117	0.0214
XC with HF exchange			
BMK	0.0112	0.0081	0.0095
M06	0.0083	0.0081	0.0082
B3LYP	0.0073	0.0046	0.0058
$BR89B94_{hyb}$	0.0205	0.0036	0.0111

Table 4
Experimentally derived D_e (eV) [16,17] and R_e (Å) [27,28] used in this work

Mol	D_e	R_e	Mol	D_e	Mol	Bond	R_e
H_2	4.75	0.7414	HCN	13.52	HCN	C–N	1.1534
N_2	9.91	1.0977	H_2O	10.07		C–H	1.0653
F_2	1.67	1.4124	H_2S	7.91	H_2O	O–H	0.9572
O_2	5.23	1.2075	CO_2	16.87	H_2S	S–H	1.3282
S_2	4.41	1.8892	NH_3	12.90	CO_2	C–O	1.1601
P_2	5.08	1.8934	PH_3	10.48	NH_3	N–H	1.0116
Cl_2	2.51	1.9870	N_2O	11.73	PH_3	P–H	1.4200
HF	6.11	0.9169	H_2O_2	11.65	N_2O	N–N	1.1284
CO	11.24	1.1283	SiH_4	13.94		N–O	1.1841
NO	6.63	1.1508	CH_4	18.18	H_2O_2	O–O	1.4556
PN	6.22	1.4909	C_2H_2	17.58		O–H	0.9619
CN	7.85	1.1718	C_2H_4	24.40	SiH_4	Si–H	1.4811
NH	3.62	1.0362	C_2H_6	30.82	CH_4	C–H	1.0859
CS	7.43	1.5349	H_2CO	16.20	C_2H_4	C–H	1.0807
CH	3.63	1.1199	CH_3OH	22.20		C–C	1.3307
OH	4.61	0.9697	C_6H_6	59.24	C_2H_2	C–H	1.0608
HCl	4.61	1.2746	C_4H_6	43.85		C–C	1.2037
SiO	8.34	1.5097	C_4H_5N	46.42	C_2H_6	C–C	1.5326
NaCl	4.25	2.3608	C_5H_5N	53.62	H_2CO	C–H	1.1007
NaF	4.98	1.9259				C–O	1.2047
					CH_3OH	C–H	1.0936
						O–H	0.9451
						C–O	1.4246
					C_6H_6	C–H	1.0831
						C–C	1.3964

R_e includes vibrational, and ro-vibrational corrections whenever available [18].

a slightly larger MAE than the meta-GGA functional BtLap reported recently [14]. These three functionals do not involve exact exchange. We used here the original parameterization of BR89B94 [9] that was based on post-LDA calculations at experimental geometries. We expect that a slight re-scaling of the two fitting parameters of this scheme would improve the accuracy further. A one-parameter hybrid scheme based on the BR89B94 functional ($BR89B94_{hyb}$) was also suggested in Ref. [9], used in a post-LDA manner

$$E_{xc} = 0.154E_{X\_exact} + 0.846E_{X\_BR89} + 1.0E_{C\_B94}. \quad (28)$$

To optimize this hybrid scheme, Becke re-scaled slightly the expression of the opposite-spin correlation length, Eq. (26) [9]

$$z_{\alpha\beta} = 0.66(R^{\alpha}_{F} + R^{\beta}_{F}). \quad (29)$$

Results with $BR89B94_{hyb}$ implemented in a SCF manner are given in Table 3. Regarding atomization energies, this somewhat forgotten hybrid scheme yields the most accurate estimates on this test set. More extended tests on a large variety of systems are ongoing and will be reported later. Note that $BR89B94_{hyb}$ has only three fitting parameters, one mixing parameter and two in the B94 correlation. B3LYP has eight parameters, while BMK and M06 are interpolation hybrid schemes with 17 parameters.

Regarding the bond distances in Table 3, the performance of the BR89B94 scheme is not so satisfactory, causing a noticeable elongation of some of the diatomic bond lengths (S_2, NaF, NaCl, NO, Cl_2). Since the parameters of this functional were optimized only on relative energies [9], some re-parameterization is required to improve the geometry estimates. The hybrid extension of this functional however, gives much better accuracy in this respect. Although its MAE is somewhat larger than the other hybrid functionals presented in Table 3, the $BR89B94_{hyb}$ functional is still better than the pure DFT schemes tested here. The above mentioned diatomic bond lengths present a difficulty for $BR89B94_{hyb}$ as well, the reasons for which are currently under scrutiny.

In conclusion, we derived and implemented for the first time a highly accurate analytical representation of the BR89B94 meta-GGA exchange–correlation scheme. It allows us to explore more fully its capabilities and leads to somewhat more robust implementation. Using the original parameterization of Ref. [9] we find that the accuracy of this functional is reasonable as far as atomization energies concern, but not so good for geometry estimates. However, the one-parameter hybrid extension of it yields the best atomization energies compared to some popular current functionals. The geometry estimates with $BR89B94_{hyb}$ are an improvement over the nonhybrid version of it, with the exception of a few diatomic molecules.

Acknowledgments

This work is supported by NIH Grant 1R43GM081928-01. The authors wish to thank David Brittain for his constructive comments on the manuscript. The authors also wish to thank Dr. Nicholas Russ for technical assistance.

Appendix

The proposed analytical form of the exchange functional BR89 can be summarized as (following Eq. (8))

$$U_{X\sigma}(\mathbf{r}) = -2\pi^{1/3}\rho^{1/3}\left(\frac{e^{x_\sigma/3}}{x_\sigma}\right)\left[1 - e^{-x_\sigma} - \frac{1}{2}x_\sigma e^{-x_\sigma}\right], \quad (A.1)$$

$$x_\sigma = g(y_\sigma)\frac{P_1(y_\sigma)}{P_2(y_\sigma)}, \quad y_\sigma(x) \equiv \frac{2}{3}\pi^{2/3}\frac{\rho_\sigma^{5/3}}{Q_\sigma}, \quad (A.2)$$

where

$$g(y) = -\arctan(a_1 y + a_2) + a_3, \quad -\infty \leqslant y \leqslant 0, \quad (A.3)$$

$$P_1(y) = \sum_{i=0}^{5} c_i y^i; \quad P_2(y) = \sum_{i=0}^{5} b_i y^i, \quad -\infty \leqslant y \leqslant 0; \quad (A.4)$$

$$g(y) = \operatorname{arccsch}(By) + 2, \quad 0 < y \leqslant +\infty,$$
$$B = 2.085749716493756 \quad (A.5)$$

$$P_1(y) = \sum_{i=0}^{5} d_i y^i; \quad P_2(y) = \sum_{i=0}^{5} e_i y^i, \quad 0 < y \leqslant +\infty. \quad (A.6)$$

The values of the coefficients a_i entering Eqs. (17) and (A.3) read

$a_1 = 1.5255251812009530,$
$a_2 = 0.4576575543602858,$
$a_3 = 0.4292036732051034.$

The values of the coefficients c_i and b_i entering Eqs. (18) and (A.4) read

$c_0 = 0.7566445420735584, \quad b_0 = 0.4771976183772063,$
$c_1 = -2.6363977871370960, \quad b_1 = -1.7799813494556270,$
$c_2 = 5.4745159964232880, \quad b_2 = 3.8433841862302150,$
$c_3 = -12.657308127108290, \quad b_3 = -9.5912050880518490,$
$c_4 = 4.1250584725121360, \quad b_4 = 2.1730180285916720,$
$c_5 = -30.425133957163840, \quad b_5 = -30.425133851603660.$

The values of the coefficients d_i and e_i entering Eqs. (23) and (A.6) read

$d_0 = 0.00004435009886795587, \quad e_0 = 0.00003347285060926091,$
$d_1 = 0.58128653604457910, \quad e_1 = 0.47917931023971350,$
$d_2 = 66.742764515940610, \quad e_2 = 62.392268338574240,$
$d_3 = 434.26780897229770, \quad e_3 = 463.14816427938120,$
$d_4 = 824.7765766052239000, \quad e_4 = 785.2360350104029000,$
$d_5 = 1657.9652731582120, \quad e_5 = 1657.962968223273000000.$

References

[1] A.D. Becke, M.R. Roussel, Phys. Rev. A 39 (1989) 3761.
[2] A.D. Becke, J. Chem. Phys. 119 (2003) 2972.
[3] A.D. Becke, J. Chem. Phys. 122 (2005) 064101.
[4] A.D. Becke, E.R. Johnson, J. Chem. Phys. 123 (2005) 154101.
[5] R. Neumann, R.H. Nobes, N.C. Handy, Mol. Phys. 87 (1996) 1.
[6] P.M.W. Gill, J.A. Pople, Phys. Rev. a 47 (1993) 2383.
[7] A.V. Arbuznikov, M. Kaupp, J. Mol. Struct. (Theochem) 762 (2006) 151.
[8] M. Abramowitz, I.A. Stegun (Eds.), Handbook of Mathematical Functions with Formulas, Graphs, and Mathematical Tables, ninth edn., Dover, New York, 1972, p. 881.
[9] A.D. Becke, Int. J. Quantum Chem. Symp. 28 (1994) 625.
[10] J.P. Perdew, Y. Wang, Phys. Rev.B 33 (1986) 8822.
[11] Y. Shao et al., Phys. Chem. Chem. Phys. 8 (2006) 3172.
[12] L.A. Curtiss, K. Raghavachari, P.C. Redfern, V. Rassolov, J.A. Pople, J. Chem. Phys. 109 (1998) 7764.
[13] L.A. Curtiss, P.C. Redfern, V. Rassolov, G.S. Kedziora, J.A. Pople, J. Chem. Phys. 22 (2001) 976.
[14] E. Proynov, J. Kong, J. Chem. Theor. Comp. 3 (2007) 746.
[15] A.J. Cohen, N.C. Handy, Mol. Phys. 99 (2001) 607.
[16] E. Clementi, S. Chakravorty, J. Chem. Phys. 93 (1990) 2591.
[17] S.A. Kafafi, J. Phys. Chem. 102 (1998) 10404.
[18] K.L. Bak, J. Gauss, P. Jorgensen, J. Olsen, T. Helgaker, J.F. Stanton, J. Chem. Phys. 114 (2001) 6548.
[19] E.I. Proynov, A.J. Thakkar, Int. J. Quantum Chem. 106 (2006) 436.
[20] A.D. Becke, Phys. Rev. A 38 (1988) 3098.
[21] C. Lee, W. Yang, R.G. Parr, Phys. Rev. B 37 (1988) 785.
[22] A.D. Becke, J. Chem. Phys. 98 (1993) 1372.
[23] P.J. Stephens, F.J. Devlin, C.F. Chabalowski, M.J. Frisch, J. Phys. Chem. 98 (1994) 11623.
[24] A.D. Boese, J.M.L. Martin, J. Chem. Phys. 121 (2004) 3405.
[25] Y. Zhao, D.G. Truhlar, J. Chem. Phys. 125 (2006) 194101.
[26] Y. Zhao, D.G. Truhlar, J. Phys. Chem. A 110 (2006) 13126.
[27] K.P. Huber, G. Herzberg, Molecular Spectra and Molecular Structure IVConstants of Diatomic Molecules, Van Nostrand Reinhold, New York, 1979.
[28] Landolt-Börnstein, Numerical Data and Functional Relationships in Science and Technology, Group II, in: K.H. Hellwege, A.M. Hellwege (Eds.), Structure Data of Free Polyatomic Molecules, vol. 7, Springer-Verlag, Berlin, 1979.